Electrically Sensing Characteristics of the Sagnac Interferometer Embedded with a Liquid Crystal-Infiltrated Photonic Crystal Fiber

Qiang Liu, Pingsheng Xue, Qiang Wu, Chenyu Zhao, Wai Pang Ng, *Senior Member, IEEE*, Yongqing Fu, and Richard Binns

***Abstract*—The electrically sensing characteristics of a liquid-crystal-infiltrated polarization-maintaining photonic crystal fiber have been studied. The small holes on the end face of the fiber collapse and two large holes remain open by controlling discharging-time, -current and -position of a fiber splicer, then liquid crystal is selectively infiltrated into the two large holes which can not only save liquid crystal, but also make the welding between the liquid-crystal-infiltrated polarization-maintaining photonic crystal fiber and single-mode fiber much easier. A new method to weld the two fibers is proposed by filling and volatilizing ethanol to make liquid crystal a few millimeters away from the end face which can improve the sensing system stability and prevent the discharge of a fiber splicer from destroying LC molecules. A Sagnac interferometer is set up by embedding the liquid-crystal-infiltrated polarization-maintaining photonic crystal fiber in a fiber loop and then its electroresponse characteristics are studied. The refractive-index distribution of the liquid-crystal-infiltrated polarization-maintaining photonic crystal fiber varies with electric voltage due to the variable index of liquid crystal which makes it possible to detect voltage. Three voltage ranges are discussed by the different dips and the sensitivity is improved with voltage increasing. The high sensitivity is up to 3.49 nm/V with the tuning range of 7 nm as voltage changes from 149.67 to 151.61 V. The Sagnac interferometer embedded with a liquid-crystal-infiltrated polarization-maintaining photonic crystal fiber can be utilized as a voltage sensor, electro-optical modulator or filter.**

***Index Terms*—Liquid crystal; Photonic crystal fiber; Sagnac interferometer; Voltage sensor; Modulator.**

I. Introduction

PHOTONIC crystal fibers (PCFs) [1]–[5], which possess many air columns, can be infiltrated with some functional materials, therefore the guided modes can be modulated which provides a way to realize many optical devices such as fiber sensors [6], [7], optical filters [8], [9], polarization splitters [10] and light sources [11]. Especially, a great number of researches for the sensors based on PCF infiltrated with environmentally sensitive materials have been studied in the last decade. Those fiber sensors are quick in response, compact in size and possess high sensitivity.

The measurement of voltage or electric field plays a significant role to detect fault and monitor state of many facilities in the fields such as medical treatment, intelligent grid, telecom, transport, chemical industry production [12]–[14]. Voltage sensors have been studied by many methods like piezoelectric effect, electrostrictive effect, Pockels effect or other physical effect [14]–[24], while they usually comprise a large bulk crystal, ceramic and polymer which lead them to have some drawbacks, such as heavy weight, large size and poor stability, making the sensors unsuitable for voltage detection in hardly-accessible environments.

Liquid crystal (LC) [25], [26] has the photoelectric characteristics and is sensitive to electric field. Once electric field above a threshold intensity is applied to nematic LC, its molecules will rotate toward the electric field direction [27], meanwhile nematic LC possesses the fluidity of liquid, therefore it can be infiltrated into the air holes of PCF. The birefringence characteristics of nematic LC-infiltrated PCF change with external electric field and its transmission spectrum will vary, therefore it can be utilized to detect voltage or electric field. This intrinsic fiber-optic sensors possess the advantages of lighter weight, smaller size and higher stability compared with the voltage sensors based on external bulk electro-optical materials.

We realized a Sagnac voltage sensor based on a high-index PCF infiltrated with LC and the sensitivity was up to -7.37 nm/V, but the results were only based on simulation [28]. An electrically tunable Sagnac filter based on a photonic bandgap fiber infused with LC was proposed and its sensitivity was 0.53 nm/V, however the PCF was entirely filled with LC which increased the difficulty of welding between PCF and single mode fiber (SMF), and leaded the discharge of a fiber splicer to destroy LC molecules easily [29]. Huang et al. also realized a high-sensitivity voltage sensor based on a PCF with one hole infiltrated with LC, but the infiltrating method was complicated by using a femtosecond laser and a three-dimensional translation stage which are expensive [30]. An electrically tunable microresonator based on LC-infiltrated PCF was realized with a high Q-factor, while its sensitivity was only 0.01 nm/V and the LC-infiltrated PCF was just

This work was supported by the National Natural Science Foundation of China (Grant No. 51907017), Natural Science Foundation of Hebei Province (Grand No. F2020501040), Key Science and Technology Research Projects of Higher Education Institutions in Hebei Province of China (Grant No. ZD2019304), Fundamental Research Funds for the Central Universities of China (Grant No. N2123012), and China National Fund for Studying Abroad.

Q. Liu, P. Xue, and C. Zhao are with Hebei Key Laboratory of Micro-Nano Precision Optical Sensing and Measurement Technology, School of Control Engineering, Northeastern University at Qinhuangdao, 066004, Peoples Republic of China (e-mail: liuqiang@neuq.edu.cn; 1901906@stu.neu.edu.cn; 1871708@stu.neu.edu.cn).

Q. Wu, W. P. Ng, Y. Fu, and R. Binns are with Faculty of Engineering and Environment, Northumbria University, Newcastle Upon Tyne, NE1 8ST, United Kingdom (e-mail: qiang.wu@northumbria.ac.uk; wai-pang.ng@northumbria.ac.uk; richard.fu@northumbria.ac.uk; richard.binns@northumbria.ac.uk).

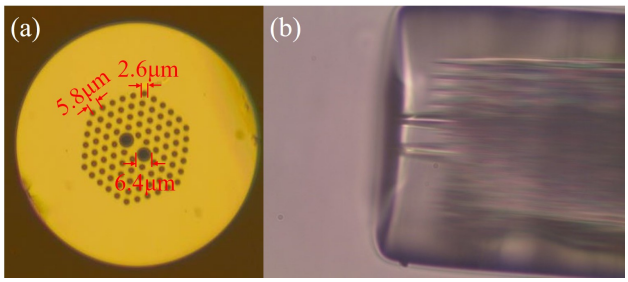

Fig. 1. (a) Cross section of the PMPCF. (b) The small air holes collapse and two large air holes remain open by controlling discharging-time, -current and -position of a fiber fusion splicer.

served as an optical microcavity, not connecting with light source and analyzer directly, which lowered its stability [31]. Mathews studied the electrically response characteristics of a PCF selectively infiltrated with LC [32]–[34], while light through the infiltrated end was collected by butt-coupling with a SMF, the special fiber was not fused with a SMF by a fiber splicer, which reduced the system stability, meanwhile the light intensity variation based sensors are easily affected by external environment and require the light source with high stability. Therefore realizing a voltage sensor with easy fabrication, high sensitivity and good stability ia necessary.

In this paper, the electrically sensing characteristics of a Sagnac interferometer embedded with a LC-infiltrated polarization-maintaining PCF (PMPCF) have been demonstrated. The small air holes collapse and two large air holes remain open by a fiber splicer not needing to utilize expensive equipment, then LC is selectively infiltrated into PMPCF by capillary effect which means the fiber-optic probe is easy to fabricate. Selective infiltration can not only save infiltrated materials, but also make the welding process easy to operate. A new method to splice the LC-infiltrated PMPCF and SMFs is proposed for the first time by filling and volatilizing ethanol to push LC a few millimeters away from the end face, which can improve the sensing system stability and prevent the discharge of a fiber splicer from destroying LC molecules. Three voltage ranges are analyzed by different dips and the corresponding sensitivities are discussed respectively. As the voltage varies from 149.67 to 151.61 V, the average sensitivity is up to 3.49 nm/V with the tuning range of 7 nm. Its repeatability, stability and response speed are also studied. This sensor with easy preparation, high sensitivity, good stability and quick response, is competitive and can also be utilized as an electro-optical modulator or filter.

II. Structure and Materials

A PMPCF-125-03 (Shanghai Fsphotonics Technology Ltd, China) which has two-dimensional symmetric structure is used in our experiment. The cross section of the special fiber is shown in Fig. 1(a). Many air holes are distributed on the cross section in triangular lattice and go through the whole fiber. This provides an opportunity to integrate optical fiber with functional materials which can be infiltrated into the air holes, and strong interaction between lightwave and matter can be realized by this way. The diameter of two air holes (6.4 μm) is larger than that of the other air holes (2.6 μm). The lattice size is 5.8 μm. The background material of this PCF is silica glass. In this paper, nematic LC is filled into the large air holes.

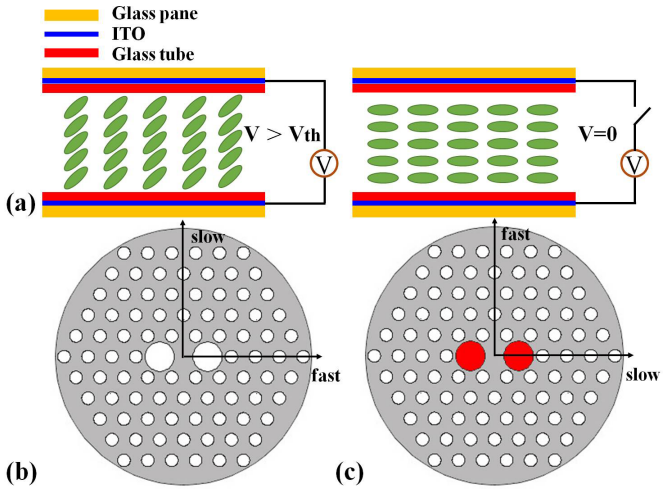

Fig. 2. (a) The state of LC molecules with and without electric field. Fast- and slow-axis in (b) empty and (c) LC-infiltrated PMPCF.

LC is selectively infiltrated into the two large holes by the following steps. First, the small holes collapse by controlling discharging-time, -current and -position of a fiber splicer (FITEL S179, FURUKAWA, Japan), while the two large holes remain open though their sizes decrease which is shown in Fig. 1(b), then LC is infiltrated into the large air holes by capillary force. Lastly, the collapsed section is cleaved off by a fiber cleaver. The length of the PMPCF is ~4 cm and the LC-infiltrated length is ~5 mm. More detailed fabrication processes of the sensing probe will be discussed in section IV.

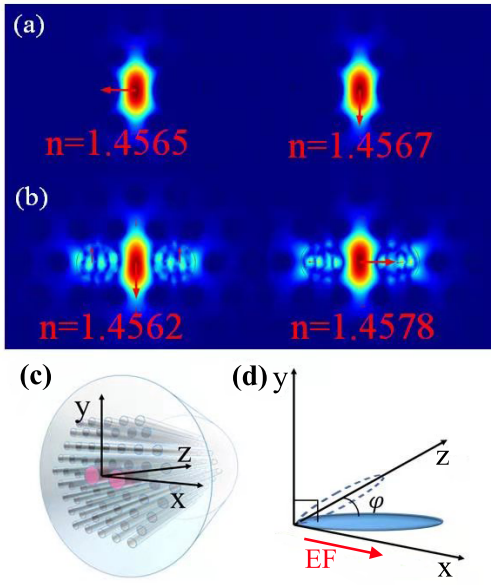

Fig. 3. x- and y-polarization modes (a) before and (b) after infiltrating LC, arrows represent the polarization directions of the modes. (c) Three-dimensional PMPCF. (d) Rotation effect of the LC molecules as the EF is in x direction.

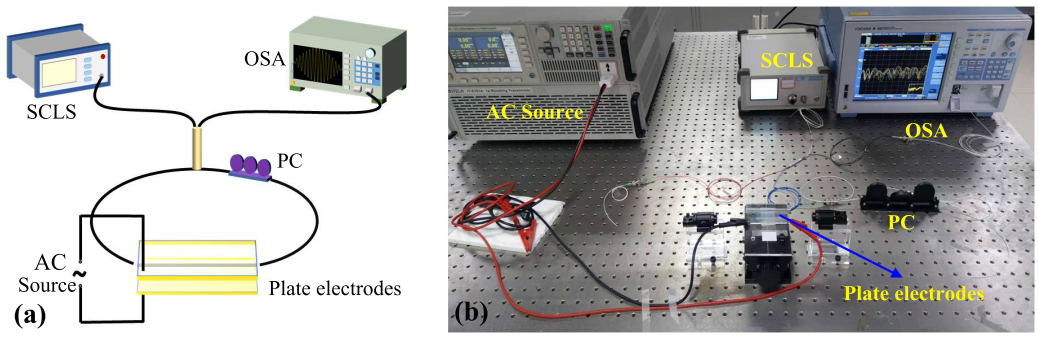

Fig. 4. (a) The schematic diagram of the fiber sensor based on a Sagnac interferometer and (b) the experimental setup.

Nematic LC is a kind of anisotropic material whose ordinary- and extraordinary-index can be represented by n_{o} and n_{e} which are higher than the refractive index of silica glass. The nematic LC used in our experiment is commercially available E7 liquid crystal with n_{o}=1.518, n_{e}=1.741 at ~20 °C (Suzhou King Optronics Co., Ltd, China). There is an electric field threshold for LC molecules to overcome anchoring energy and reorient in the holes, LC molecules will rotate toward the electric field direction as the electric field intensity around the fiber is above the threshold, then the index distribution of the PMPCF varies which leads its transmission modes to change.

III. Principle and Experimental Setup

The LC molecules rotate as an electric field is applied (Fig. 2(a)), the rotation angle can be represented by [35]:

$$\varphi = \begin{cases} 0 & E \le E_C \\ \frac{\pi}{2} - 2\tan^{-1}\left[\exp\left(-\frac{E-E_C}{30E_C}\right)\right] & E > E_C \end{cases}, \quad (1)$$

E_C represents the electric field threshold, LC molecules start to rotate as the electric field exceeds this value. The relation between the permittivity $\varepsilon = [\varepsilon_{xx}, \varepsilon_{yy}, \varepsilon_{zz}]$ and rotation angle can be represented by $\varepsilon_{xx} = \varepsilon_e \sin^2\varphi + \varepsilon_o \cos^2\varphi, \varepsilon_{yy} = \varepsilon_o, \varepsilon_{zz} = \varepsilon_o \sin^2\varphi + \varepsilon_e \cos^2\varphi$ when the electric field is applied in x direction [36]. The refractive index of x-polarization mode increases with electric field while that of y-polarization mode is almost constant.

The two large holes of the PMPCF create strong birefringence. The birefringence axes without LC are shown in Fig. 2(b). We usually name these two axes as fast- (crossing the centers of two large holes) and slow-axis (the vertical direction to the fast axis). The fast-axis direction has a lower refractive index than that of the slow-axis direction due to the two large air holes, therefore the velocity of light in the fast-axis direction is higher. The fast- and slow-axis of the fiber interchange after selectively infiltrating LC with high index into the two large holes (Fig. 2(c)). The mode field distributions and effective refractive indices are calculated by finite element method. Perfectly matched layer, for which cylindrical coordinate is utilized, is set to absorb radiant energy from fiber core. Meanwhile, the outer boundary of perfectly matched layer is set as scattering boundary condition which can prevent from reflecting energy which may disturb fiber transmission mode. The parameters of PMPCF structure is shown in Fig. 1(a). The triangular sub-domain is applied to discretize the computation region which is meshed into 12429 elements. Fig. 3(a) and (b) show x- and y-polarization modes at the wavelength of 1440 nm before and after infiltrating LC, the fast- and slow-axis interchange after LC is infiltrated. Fig. 3(c) shows the three-dimensional PMPCF and (d) shows the rotation effect of LC molecules as the electric field (EF) is in x direction.

Figure 4 shows (a) the schematic diagram of the fiber sensor based on a Sagnac interferometer and (b) the experimental setup. The sensing fiber is kept straight and stable by fiber fixtures. One beam of light from a supercontinuous light source (SCLS) is equally split into two beams by a 3 dB optical coupler which propagate in clockwise- and counterclockwise-direction in the fiber loop. Due to the birefringence characteristics of the LC-infiltrated PMPCF, there is a phase difference between the two beams as they transmit back to the coupler where interference will occur. Polarization controller (PC) is utilized to control the polarization state of light to optimize interference fringes. As the two large holes are filled with nematic LC, the birefringence of the PMPCF can be modulated by electric field, and the interferometric fringes will shift with electric field.

For the Sagnac interferometer, transmittance can be calculated by [37], [38]:

$$T = \frac{1 - cos(2\pi BL/\lambda)}{2}, \quad (2)$$

where L represents the length of PMPCF and the birefringence $B = |n_{\mathrm{fast}} - n_{\mathrm{slow}}|$. The dips appear in output spectrum as $2\pi BL/\lambda$=$2m\pi$, m is an integer.

The light source (SC-5, Wuhan Yangtze Soton Laser Co., Ltd, China) is utilized in the experiment. Transmission spectrum is recorded by an optical spectrum analyzer (OSA) (AQ6370D, YOKOGAWA, Japan). We set the LC-infiltrated PMPCF between two pieces of ITO (indium tin oxide) glass which are used as electrodes. The distance between the two pieces of ITO glass is ~330 μm and the parallel electric field is generated perpendicularly to the fiber axis. An AC source is utilized that provides a positive polarity voltage waveform with 1 kHz of sinusoidal electrical signal which means that the voltage changes continuously with respect to time, while it changes such fast that the OSA can't detect this change and the effective value of the voltage is at an equilibrium level. The

spectrum displayed on the OSA is stable as the maximum of a sinusoidal voltage is fixed and the voltage sensed by the LC molecules is the effective value. In addition, a multimeter is utilized to test the accuracy of our system and the error is within 0.01 V. DC source is not used due to that it can lead to deterioration of LC performance as LC is exposed to DC voltage for a long time [34]. The experimental equipment for this voltage sensing system mainly includes OSA whose size is large (the length: 459 mm, width: 426 mm and height: 221 mm) and SCLS, however they can be reduced in size with the development of science and technology, then a portable voltage sensing system would be realized.

IV. Sensing Probe Fabrication

The two ends of a LC-infiltrated PMPCF are spliced with two SMFs respectively and then the special fiber can be embedded in a Sagnac loop. If there is no further post-processing after LC is infiltrated, the arc discharge of a fusion splicer would destroy LC molecules near the end face of the special fiber. Most previous experiments for the LC-infiltrated PCF tried to avoid this by face-to-face coupling which means that the end face of the LC-infiltrated fiber is simply in touch with the end face of the SMF in line without splicing. The method of face-to-face coupling is effective as one beam of light transmits to OSA directly while the system stability decreases, while face-to-face coupling is no longer appropriate for Sagnac interferometer because the light reflected on the fiber face will interfere output spectrum. Therefore, some proper operations are necessary to splice the LC-infiltrated PCF and SMF to increase the sensing system stability and avoid destroying LC molecules.

The whole operation procedures to fabricate sensing probe are shown in Fig. 5. First, the small air holes collapse and the two large holes remain open by controlling discharging-time, -current and -position of a fiber splicer, the discharging time is 20 ms, the discharging current is 80 mA and the fiber end is 50 μm away from the discharging electrodes. After LC is infiltrated in the large holes, it is pushed several millimeters

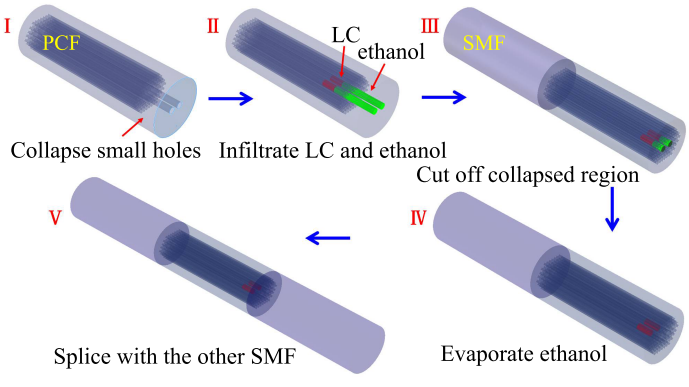

Fig. 5. The whole operation procedures to fabricate sensing probe. I. The small holes collapse and the two large holes remain open by the discharging of a fiber splicer; II. Infiltrating LC and ethanol in the large holes by capillary effect; III. Splicing the other end of PMPCF with a SMF and cutting off the collapsed region; IV. Evaporating ethanol; V. The filled end of PMPCF is spliced with the other SMF.

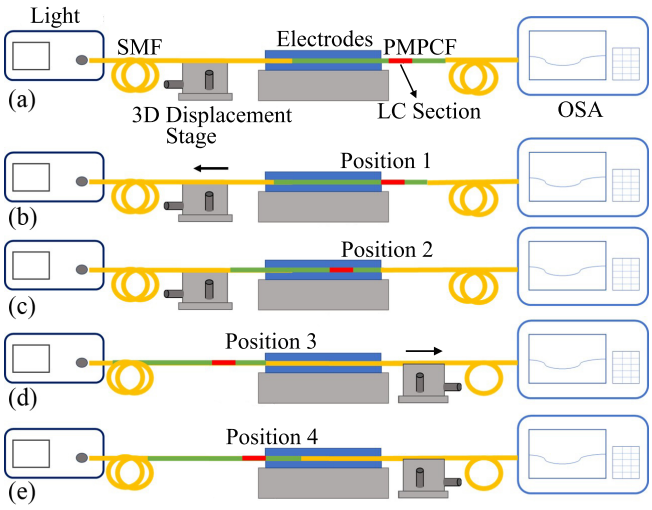

Fig. 6. The measurement procedures of the LC-infiltrated length. The green fiber is PMPCF, the yellow fiber denotes SMF and the red part represents the LC-infiltrated section. (a) Measurement setup. Moving the fibers toward left to (b) position 1 and (c) position 2. The displacement from position 1 to position 2 is L_1. Then, moving the fibers toward right to (d) position 3 and (e) position 4, and the displacement from position 3 to position 4 is L_2. The LC-infiltrated length L can be calculated by $L_1 - L_2$.

away from the end face by infiltrating a little ethanol. Then, the other end of the PMPCF is spliced with a SMF before ethanol volatilizing, the purpose of this procedure is to block the air holes on the other side of the PMPCF to avoid LC being pulled back by air pressure during ethanol volatilizing. Subsequently, the collapsed region is cut off. Then, ethanol evaporates and LC is kept a distance away from the filling end. Lastly, the filled end of the PMPCF is spliced with a SMF by a fiber fusion splicer. It needs attention that ethanol should be completely evaporated before final splicing, otherwise gas cavity would form in the fusion area due to the discharging. This method is suitable for the short infiltrated length because it will be hard to continue to fill ethanol if the LC-infiltrated section is very long.

Different PCF and LC-infiltrated lengths have been tested. The influences of PCF length on the sensitivity and loss are negligible. Increasing the length of the LC-infiltrated section, the sensitivity can be improved because the phase difference can experience more changes under the same voltage variation, however longer LC-infiltrated section will cause greater loss. The infiltrated length of a few millimeters is chosen to balance loss and sensitivity. When LC-infiltrated section is ~5 mm, the loss is about 20 dB. There are many small holes around the two large holes, the LC in the holes cannot be observed clearly and the 5 mm length is indirectly measured by following steps. The measurement setup is shown in Fig. 6(a). The green fiber is PMPCF, the yellow fiber denotes SMF and the red part represents LC-infiltrated section. A high voltage is applied to the glass electrodes. The fibers are moved slowly by a 3D displacement stage toward left until the spectrum is about to change which means the left of the LC-infiltrated section reaches the edge of electrodes which is labeled position 1 shown in Fig. 6(b). Continuing to move the fiber toward left

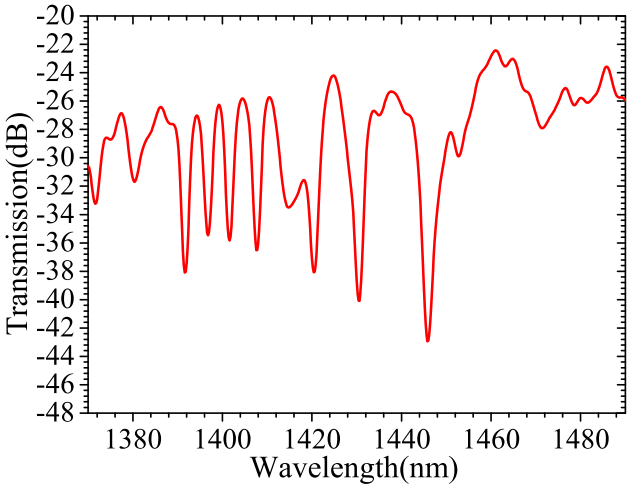

Fig. 7. Transmission spectrum of the Sagnac interferometer embedded with a LC-infiltrated PMPCF without electric field. It can be found multiple dips appear due to mode interference.

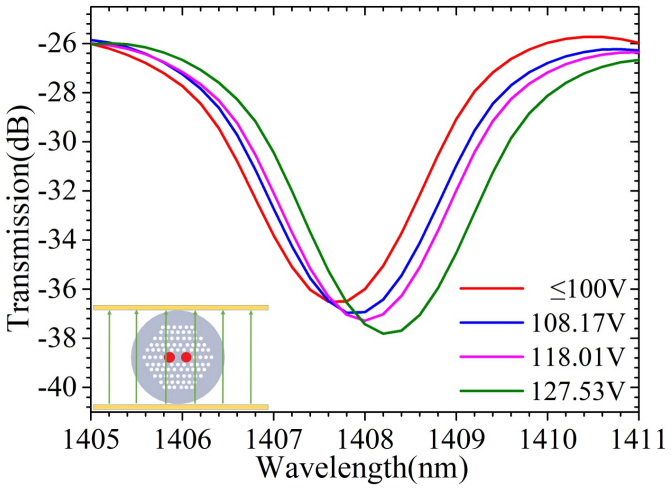

Fig. 8. Transmission spectrum with different voltages, the direction of electric field is set perpendicular to the connecting line of the two large holes' centers (inset). The dip shifts to longer wavelength with voltage increasing.

to position 2, the splicing point between the PMPCF and SMF reaches the edge of electrodes shown in Fig. 6(c). The displacement L_1 from position 1 to 2 is recorded. The same procedures are implemented to measure the displacement L_2 from position 3 in Fig. 6(d) to position 4 in Fig. 6(e). Last, the LC-infiltrated length L can be calculated by $L_1 - L_2$.

V. Results and Discussion

The spectrum shows multiple dips caused by Sagnac interference in a certain wavelength range without electric field shown in Fig. 7. A polarization controller was tuned to make the dips more apparent.

The direction of electric field is set perpendicular to the connecting line of the two large holes' centers first, as it is shown in the inset of Fig. 8. The output voltage of the AC source is increased step by step, no obvious change of the interference fringes is observed until voltage reaches 100 V. Fig. 8 shows the transmission spectrum as voltage changes

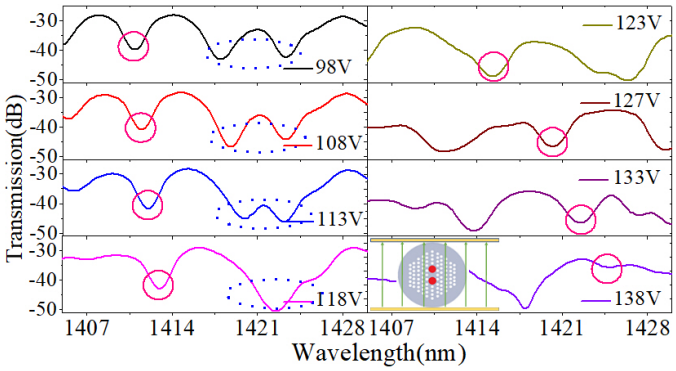

Fig. 9. Transmission spectrum with different voltages, the direction of electric field is set parallel to the connecting line of the two large holes' centers (inset). The dip marked by pink circle shifts to longer wavelength with voltage increasing and the dip contrast gets poor as voltage is 138 V.

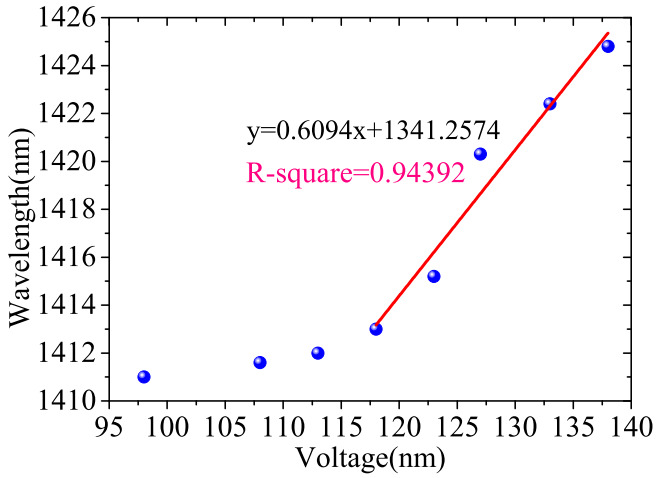

Fig. 10. Dip wavelength versus voltage which varies from 98 to 138 V. It can be seen the shift is not obvious at low voltages and the average sensitivity is 0.6094 nm/V as voltage increases from 118 to 138 V.

from 100 to 127.53 V. As the voltage increases, the dips could be found red shifted slightly and the dip shifts from 1407.6 to 1408.2 nm with the sensitivity of ∼0.02 nm/V.

Then, the direction of electric field is set parallel to the connecting line of the two holes' centers, as the inset in Fig. 9 shows. The threshold voltage of the LC-infiltrated PMPCF is ∼98 V which is a little different from 100 V obtained in last case because the light path changes slightly as rotating the special fiber. The sensitivity is higher than that the electric field is set perpendicular to the direction as shown in Fig. 8. Spectrum red shifts continuously as voltage increases from 98 to 138 V shown in Fig. 9, the dip marked by pink circle shifts from 1411 to 1424.8 nm and the shift is not obvious at low voltages until voltage reaches about 118 V because LC molecules need to overcome the effect of thermal motion and anchoring energy, and start to tilt as the voltage is just over the threshold value. This also can be obtained from the dip wavelength versus voltage shown in Fig. 10. The tilt angle of LC molecules versus voltage is not linear presented in [28], the wavelength shift with voltage will not be linear, while it can be considered linear in a limited range. From Fig. 9 we can see

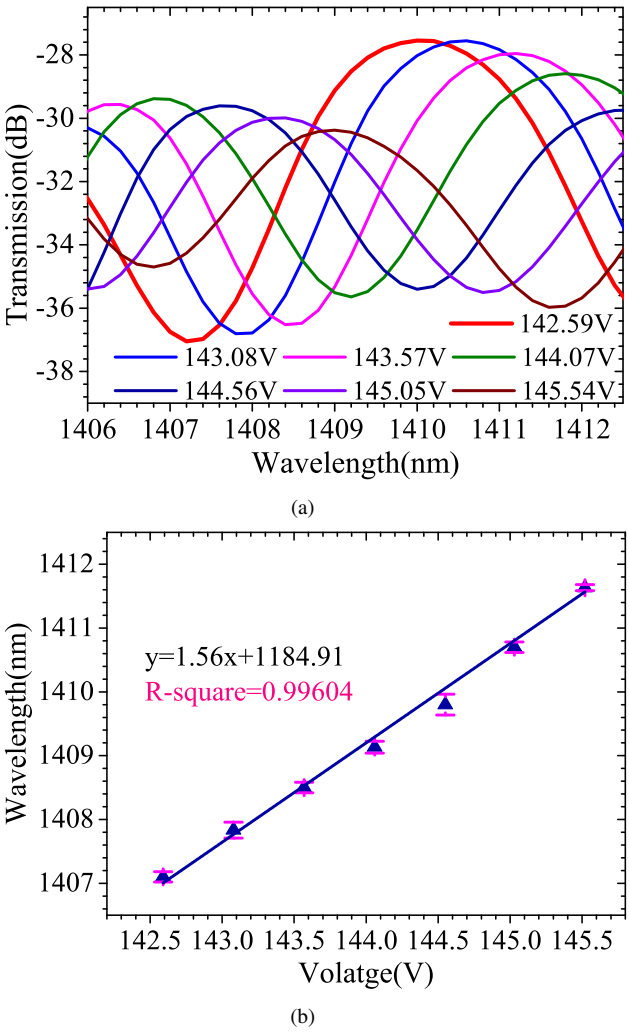

Fig. 11. (a) Transmission spectrum as voltage changes from 142.59 to 145.54 V. The direction of electric field is set parallel to the connecting line of the two large holes' centers. (b) The relation between dip wavelength and voltage. The slope of fitted line reveals its average sensitivity of 1.56 nm/V with the linearity of 0.99604. And the linear fitting is performed with 4 groups of repeated experiments.

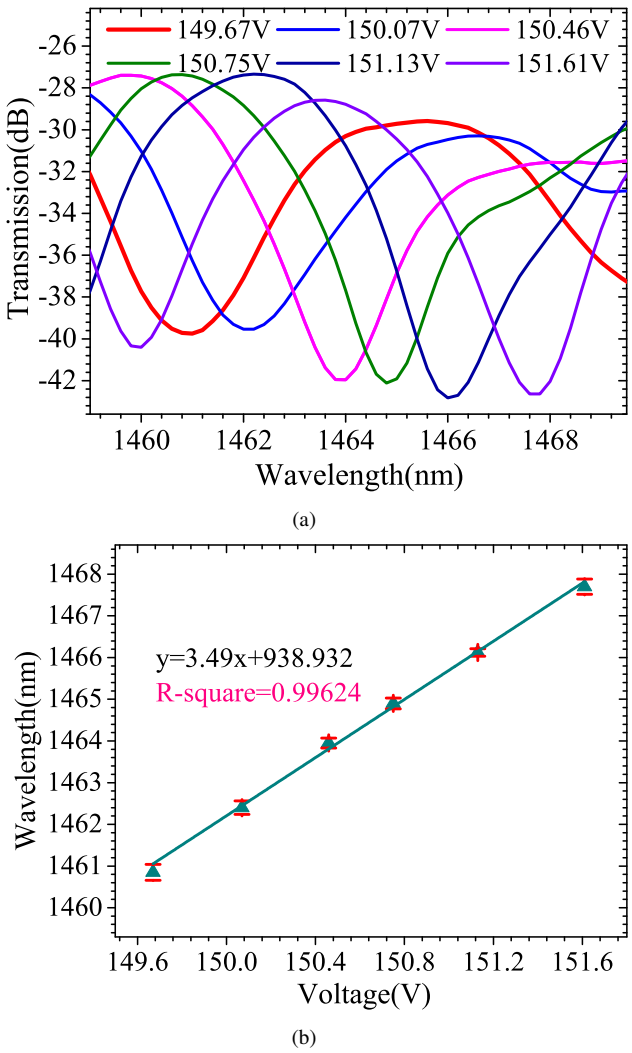

Fig. 12. (a) Transmission spectrum as voltage changes from 149.67 to 151.61 V. The direction of electric field is set parallel to the connecting line of the two holes' centers. (b) The relation between dip wavelength and voltage. The linear fitting is performed with 5 groups of repeated experiments and its average sensitivity is up to 3.49 nm/V with the linearity of 0.99624.

the dip contrast gets poor as voltage is 138 V which restricts the ability to continue tracking the dip and realize a wide detection range. The linear fit is made as voltage varies from 118 to 138 V and the fitting equation is y=0.6094x+1341.2574. The sensitivity is 0.6094 nm/V, the detection range is 20 V and its linearity is 0.94392. We also find two dips marked by blue ellipse merge to form a dip as voltage changes from 98 to 118 V which has been explained in [6], [7]. Then the different dips, which are relatively obvious for measurement, are tracked to explore the sensing characteristics of the LC-infiltrated PMPCF at higher voltages.

One different dip is recorded as voltage changes from 142.59 to 145.54 V. The direction of electric field is set parallel to the connecting line of the two holes' centers. The dip shifts 4.5 nm from 1407.2 to 1411.7 nm shown in Fig. 11(a). The relationship between the dip wavelength and voltage is linearly fitted in Fig. 11(b). The experiment is repeated four times. The fitted line indicates its average sensitivity is 1.56 nm/V and the linearity is 0.99604 in this detected range.

Then, we track another dip and find the sensitivity is improved than before as voltage varies from 149.67 to 151.61 V. Fig. 12(a) shows the corresponding transmission spectrum and the dip shifts 7 nm. The dip wavelength dependent on voltage is shown in Fig. 12(b). The experiment is repeated five times. The average sensitivity is improved to 3.49 nm/V and the linearity is as high as 0.99624. Compared with the three voltage ranges, the sensitivity increases with voltage we think this is because the LC molecules are tilted more evenly under a higher voltage. The fiber voltage sensor exhibits high sensitivity and the linearity is good in a limited detection range. The detection range is narrow because the free spectrum range (FSR) is not enough high and the tracked dips would disappear as the voltage increases to a value. In the future research, we will focus on the method to improve the dynamic detection range of the LC-infiltrated PCF based sensors to satisfy practical applications. From the error bars in Fig. 11(b) and Fig. 12(b), it can be seen the repeatability is satisfactory,

TABLE I
PERFORMANCE COMPARISONS BETWEEN OURS AND PREVIOUS WORKS

Ref.	LC	Infiltration	Fiber	Sensitivity
[29]	MDA	Full	PCF	0.53nm/V
[31]	BHR	Full	PCF	0.01nm/V
[33]	MDA-MLC	Selective	PCF	2.2dB/kV/mm
[39]	NLC	Full	PCF	4.55dB/kV/mm
[40]	MLC	Full	PCF	<1.57nm/V
[41]	E7	Full	PCF	0.445dB/V
[42]	E7	Full	PCF	1.8nm/V
[43]	5CB	–	TFBG	1.148dB/V
[44]	E7	Full	HCF	1.225nm/V
[45]	LC	Full	PCF	10.5nm/kV/mm
Ours	E7	Selective	PCF	3.49nm/V (1151.7nm/kV/mm)

(HCF: hollow-core fiber, TFBG: tilted fiber Bragg grating, Infiltration: infiltration style.)

the maximum standard deviations for the two voltage ranges are 0.1633 nm at 144.56 V and 0.19149 nm at 149.67 V. Ambient temperature, vibration, optical fiber deformation such as torsion, stretch are the possible error sources for this proposed sensing system. Voltage U=E·D where D represents the distance between two electrodes. Threshold electric field is a certain value for this E7-infiltrated PMPCF, therefore threshold voltage can be changed by modulating the distance D. The voltage sensitivity of 3.49 nm/V under the circumstances of 330 μm between two electrodes can be converted into electric field sensitivity of 1151.7 nm/kV/mm which is competitive in the field of electric field detection. Table I shows the performance comparisons between ours and previous works. The threshold voltage of this LC-infiltrated PMPCF is ∼98 V which means the minimum value of the measurable voltage is 98 V. The maximum measurable voltage is 151.61 V in this work, while the maximum can be higher than this level because this proposed sensor is essentially based on the state of LC molecules which will continue to rotate as the voltage becomes larger until the rotation angle of LC molecules is close to 90 degrees [28].

The stability of the sensor is revealed in Fig. 13. The direction of electric field is set parallel to the connecting line of the two holes' centers. The dips are recorded every 10 minutes. The dip drifts are less than 0.3 nm within 50 minutes when the voltages of 149.18 and 151.63 V are applied which demonstrates its stability is satisfactory.

To investigate the electro-optical response speed of the sensing structure, a photodetector (PDA05CF2, Thorlabs) and an oscilloscope (DSOX6002A, Keysight) are utilized to measure the response time. The 140 V, 1 kHz sinusoidal signal with switching period of 1 second is applied to the LC-infiltrated PMPCF. We find its average response time is 235.5 ms and recovery time is 34.8 ms shown in Fig. 14. It can be seen the response to a electric field is quick enough, besides used as an electrical sensor, it has the possibility to be used as an electro-optical modulator, filter or optical switch and so on.

Some authors demonstrated the electrically sensing characteristics of LC-filled PCF based on AC source in the range of ∼1 kHz [29]–[33], [39]–[42]. The literature [34] demonstrated the relation between the transmission properties of a nematic LC-filled PCF and the frequency of applied electric field, and the response time was recorded by a high-speed powermeter with frequency increasing from 50 Hz to 1 kHz. The transmission properties of LC-filled PCF depend on the frequency of applied electric field because LC molecules dynamically reorientate with the sinusoidally varying electric field and the response time can be obtained by the following equation:

$$\tau = \frac{\gamma}{[(\varepsilon_{\parallel} - \varepsilon_{\perp}) - (E^2 - E_{th}^2)]}, \tag{3}$$

where γ denotes the rotation viscosity of the NLC, $\varepsilon_{\parallel}$, $\varepsilon_{\perp}$ are the dielectric permittivities which depend on frequency, E_{th} represents threshold electric field. It can be seen the response time depends on external electric field and frequency. The literature also revealed response time τ, threshold field E_{th} decrease and the sensitivity for the electric field varying from

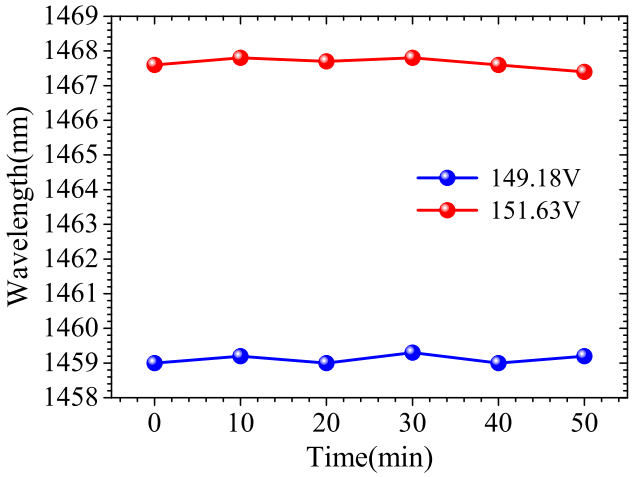

Fig. 13. Dips drift over time when the voltages of 149.18 and 151.63 V are applied. The dips are recorded every 10 minutes and the drifts are less than 0.3 nm within 50 minutes.

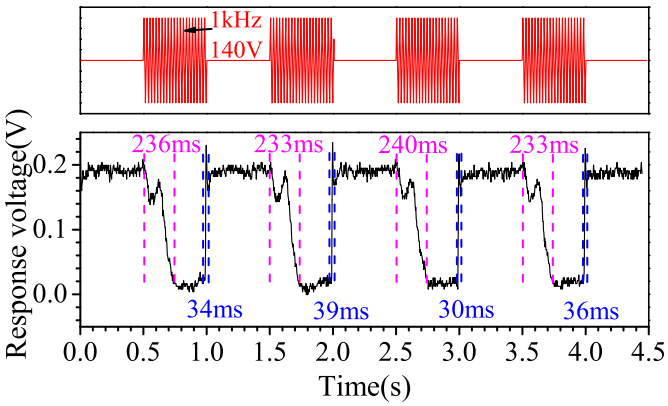

Fig. 14. Response characteristics of the LC-infiltrated PMPCF with time. Response and recovery times are measured under the electric field of 1 kHz, 140 V on and off every 0.5 s.

0 to 5.0 kV/mm increases with frequency increasing from 50 Hz to 1 kHz. Due to the ability to sense frequency, the fiber sensor can be used as a frequency monitor. In order to make our sensor more convenient for practical use, it is required to have a wide frequency range and large dynamic measurement range [46]. In the future research, we will try to improve the frequency range and dynamic measurement range for the sensors based on LC-infiltrated PCF.

VI. Conclusion

The electrically sensing characteristics of a PMPCF infiltrated with LC have been investigated. The small air holes collapse and the two large holes remain open by controlling discharging-time, -current and -position of a fiber splicer, the discharging time is 20 ms, the discharging current is 80 mA and the fiber end is 50 m away from the discharging electrodes. Then LC is selectively infiltrated into two large holes and the filling length is only ∼5 mm. We propose a new method to splice the LC-infiltrated PMPCF and SMFs by filling and evaporating ethanol to push LC a few millimeters away from the end face and avoid the discharge of a fusion splicer destroying LC molecules. In the experiment, the LC-infiltrated PMPCF is embedded in a Sagnac loop to form a Sagnac interferometer and the interference dips red shift as voltage increases. Three voltage ranges are discussed by the different dips and we find the sensitivity is improved with voltage increasing. The sensitivity is 1.56 nm/V with the tuning range of 4.5 nm as voltage varies from 142.59 to 145.54 V and the linearity is 0.99604. Meanwhile, it is up to 3.49 nm/V with the tuning range of 7 nm as voltage increases from 149.67 to 151.61 V and the linearity is 0.99624. As voltages are fixed the dip drifts are less than 0.3 nm within 50 minutes which demonstrates the sensor possesses good stability. The average response and recovery times are only 235.5 and 34.8 ms. In short, though the dynamic measurement range needs to be further improved to satisfy practical applications, this proposed fiber sensor based on LC-infiltrated PMPCF Sagnac interferometer shows many advantages, such as easy fabrication, high sensitivity, good stability and quick response.

References

[1] P. S. J. Russell, "Photonic crystal fibers," *Science*, vol. 299, no. 5605, pp. 358-362, Jan. 2003.

[2] G. K. L. Wong, M. S. Kang, H. W. Lee, F. Biancalana, C. Conti, T. Weiss, and P. S. J. Russell, "Excitation of orbital angular momentum resonances in helically twisted photonic crystal fiber," *Science*, vol. 337, no. 6093, pp. 446-449, Jul. 2012.

[3] X. Zhou, S. G. Li, X. Li, X. Yan, X. Zhang, and T. Cheng, "A vectorial analysis of the curvature sensor based on a dual-core photonic crystal fiber," *IEEE T. Instrume. Meas.*, vol. 69, no. 9, pp. 6564-6570, Sept. 2020.

[4] Q. Liu, L. Xing, Z. Wu, Y. Fu, S. Li, P. Xue, W. P. Ng, Q. Wu, and R. Binns, "Cascaded Sagnac loops embedded with two polarization maintaining photonic crystal fibers for highly sensitive strain measurement," *IEEE T. Instrume. Meas.*, vol. 70, pp. 1-9. Jan. 2021. DOI: 10.1109/TIM.2021.3050822

[5] W. Luo, X. Li, J. Meng, Y. Wang, and X. Hong, "Surface plasmon resonance sensor based on side-polished D-shaped photonic crystal fiber with split cladding air holes," *IEEE T. Instrume. Meas.*, vol. 70, pp. 1-11, Jan. 2021. DOI: 10.1109/TIM.2021.3054003

[6] Q. Liu, L. Xing, S. Yan, L. Lv, and Z. Liu, "Sensing characteristics of photonic crystal fiber Sagnac interferometer based on novel birefringence and Vernier effect," *Metrologia*, vol. 57, no. 3, p. 035002, May 2020.

[7] Q. Liu, S. G. Li, and H. Chen, "Enhanced sensitivity of temperature sensor by a PCF with a defect core based on Sagnac interferometer," *Sensor. Actuat. B-Chem.*, vol. 254, pp. 636-641, Jan. 2018.

[8] Q. Liu, S. G. Li, J. S. Li, C. Dou, X. Y. Wang, G. Y. Wang, and M. Shi, "Tunable fiber polarization filter by filling different index liquids and gold wire into photonic crystal fiber," *J. Lightwave Technol.*, vol. 34, no. 10, pp. 2484-2490, May 2016.

[9] M. Chang, B. Li, N. Chen, X. Lu, X. Zhang, and J. Xu, "A compact and broadband photonic crystal fiber polarization filter based on a plasmonic resonant thin gold film," *IEEE Photon. J.*, vol. 11, no. 2, pp. 1-12, Apr. 2019.

[10] E. Wang, H. Jiang, K. Xie, C. Chen, and Z. Hu, "Polarization splitter based on dual core liquid crystal-filled holey fiber," *J. Appl. Phys.*, vol. 120, no. 11, p. 114501, Sep. 2016.

[11] P. S. J. Russell, P. Holzer, W. Chang, A. Abdolvand, and J. C. Travers, "Hollow-core photonic crystal fibres for gas-based nonlinear optics," *Nat. Photonics*, vol. 8, no. 4, pp. 278-286, Apr. 2014.

[12] Y. Shi, W. Wang, Z. Zhu, J. Yang, X. Nie, and Y. Cheng, "A bias controllable birefringence modulation measurement system for subnanosecond pulsed electric field," *IEEE T. Instrume. Meas.*, vol. 70, pp. 1-11, Feb. 2021. DOI: 10.1109/TIM.2020.3037307

[13] Bobowski, J. S., Ferdous, M. S., and Johnson, T. "Calibrated single-contact voltage sensor for high-voltage monitoring applications," *IEEE T. Instrume. Meas.*, vol. 64, no. 4, pp. 923-934, Apr. 2014.

[14] Q. Yang, Y. He, S. Sun, M. Luo, and R. Han, "An optical fiber Bragg grating and piezoelectric ceramic voltage sensor," *Rev. Sci. Instrum.*, vol. 88, no. 10, p. 105005, Oct. 2017.

[15] H. Yang, Y. Guo, S. Jiao, W. Hong, S. Xu, and Y. Zhang, "Analysis and suppression of nonreciprocal phase shift error of the optical voltage sensor based on the converse piezoelectric effect," *Opt. Fiber Technol.*, vol. 55, p. 102142, Mar. 2020.

[16] K. Kawamura, H. Saito, and F. Noto, "Development of a high voltage sensor using a piezoelectric transducer and a strain gage," *IEEE T. Instrume. Meas.*, vol. 37, no. 4, pp. 564-568, Dec. 1988.

[17] Y. He, Q. Yang, S. Sun, M. Luo, R. Liu, and G. D. Peng, "A multi-point voltage sensing system based on PZT and FBG," *Int. J. Elec. Power.*, vol. 117, p. 105607, May 2020.

[18] R. C. Allil, and M. M. Werneck, "Optical high-voltage sensor based on fiber Bragg grating and PZT piezoelectric ceramics," *IEEE T. Instrume. Meas.*, vol. 60, no. 6, pp. 2118-2125, Jun. 2011.

[19] L. Fabiny, S. T. Vohra, and F. Bucholtz, "High-resolution fiber-optic low-frequency voltage sensor based on the electrostrictive effect," *IEEE Photon. Technol. Lett.*, vol. 5, no. 8, pp. 952-953, Aug. 1993.

[20] L. Fabiny, S. T. Vohra, and F. Bucholtz, "High resolution fiber-optic voltage sensors based on the electrostrictive effect," *Ferroelectrics*, vol. 151, no. 1, pp. 91-96, Feb. 1994.

[21] Q. Yang, R. Liu, Y. He, and M. Luo, "AC/DC hybrid electric field measurement method based on Pockels effect and electric field modulation," *Rev. Sci. Instrum.*, vol. 91, no. 5, p. 055004, May 2020.

[22] S. Choi, A. A. Sugianto, D. G. Lee, H. J. Woo, S. H. Hong, and Y. C. Ghim, "Polar-coordinate-based data analysis scheme for high-voltage measurement system using the Pockels electro-optic effect," *J. Instrum.*, vol. 15, no. 03, p. C03030, Mar. 2020.

[23] Y. Li, L. Gao, J. Wan, and J. Liu, "Optical DC electric field sensing based on the Pockels effect using bismuth germanate crystals," *Appl. Opt.*, vol. 59, no. 21, pp. 6237-6244, Jul. 2020.

[24] J. Zhang, L. Yang, and Y. Li, "Non-invasive measurement of intensive power-frequency electric field using a $LiNbO_3$-integrated optical waveguide sensor," *IET Sci. Meas. Technol.*, vol. 15, no. 1, pp. 101-108, Jan. 2021.

[25] C. P. Lapointe, T. G. Mason, and I. I. Smalyukh, "Shape-controlled colloidal interactions in nematic liquid crystals," *Science*, vol. 326, no. 5956, pp. 1083-1086, Nov. 2009.

[26] B. G. Jeon, T. H. Choi, S. M. Do, J. H. Woo, and T. H. Yoon, "Effects of curing temperature on switching between transparent and translucent states in a polymer-stabilized liquid-crystal cell," *IEEE Trans. Electron Devices*, vol. 65, no. 10, pp. 4387-4393, Oct. 2018.

[27] D. Budaszewski, M. Chychlowski, A. Budaszewska, B. Bartosewicz, B. Jankiewicz, and T. R. Wolinski, "Enhanced efficiency of electric field tunability in photonic liquid crystal fibers doped with gold nanoparticles," *Opt. Express*, vol. 27, no. 10, pp. 14260-14269, May 2019.

[28] Q. Liu, P. Xue, and Z. Liu, "Voltage sensor based on liquid-crystal-infiltrated photonic crystal fiber with high index," *Appl. Phys. Express*, vol. 13, no. 3, p. 032005, Feb. 2020.

[29] J. Du, Y. Liu, Z. Wang, B. Zou, B. Liu, and X. Dong, "Electrically tunable Sagnac filter based on a photonic bandgap fiber with liquid crystal infused," *Opt. Lett.*, vol. 33, no. 19, pp. 2215-2217, Sep. 2008.

[30] Y. Huang, Y. Wang, L. Zhang, Y. Shao, F. Zhang, C. Liao, and Y. Wang, "Tunable electro-optical modulator based on a photonic crystal fiber selectively filled with liquid crystal," *J. Lightwave Technol.*, vol. 37, no. 9, pp. 1903-1908, Jan. 2019.
[31] C. Yang, H. Zhang, B. Liu, Y. Li, and H. Liu, "Electrically tunable whispering gallery mode microresonator based on a grapefruit-microstructured optical fiber infiltrated with nematic liquid crystals," *Opt. Lett.*, vol. 42, no. 15, pp. 2988-2991, Jul. 2017.
[32] S. Mathews, G. Farrell, and Y. Semenova, "Directional electric field sensitivity of a liquid crystal infiltrated photonic crystal fiber," *IEEE Photon. Technol. Lett.*, vol. 23, no. pp. 408-410, Apr. 2011.
[33] S. Mathews, G. Farrell, and Y. Semenova, "All-fiber polarimetric electric field sensing using liquid crystal infiltrated photonic crystal fibers," *Sensor. Actuat. A-Phys.*, vol. 167, no. 1, pp. 54-59, May 2011.
[34] S. Mathews, G. Farrell, and Y. Semenova, "Experimental study on the frequency dependence of the liquid crystal infiltrated photonic crystal fibers," *IEEE Sens. J.*, vol. 12, no. 5, pp. 1018-1024, May 2011.
[35] S. Ertman, T. R. Wolinski, D. Pysz, R. Buczynski, E. Nowinowski-Kruszelnicki, and R. Dabrowski, "Low-loss propagation and continuously tunable birefringence in high-index photonic crystal fibers filled with nematic liquid crystals," *Opt. Express*, vol. 17, no. 21, pp. 19298-19310, Oct. 2009.
[36] E. L. Wang, H. M. Jiang, K. Xie, C. Chen, and Z. J. Hu, "Polarization splitter based on dual core liquid crystal-filled holey fiber," *J. Appl. Phys.*, vol.120, no. 11, pp. 114501, Sep. 2016.
[37] T. Han, Y. G. Liu, Z. Wang, J. Guo, Z. Wu, S. Wang, Z. Li, and W. Zhou, "Unique characteristics of a selective-filling photonic crystal fiber Sagnac interferometer and its application as high sensitivity sensor," *Opt. Express*, vol. 21, no. 1, pp. 122-128, Jan. 2013.
[38] Y. Liu, B. Liu, X. Feng, W. Zhang, G. Zhou, S. Yuan, G. Kai, and X. Dong, "High-birefringence fiber loop mirrors and their applications as sensors," *Appl. Opt.*, vol. 44, no. 12, pp. 2382-2390, Apr. 2005.
[39] S. Mathews, G. Farrell, and Y. Semenova, "Liquid crystal infiltrated photonic crystal fibers for electric field intensity measurements," *Appl. Opt.*, vol. 50, no. 17, pp. 2628-2635, Jun. 2011.
[40] L. Wei, T. T. Alkeskjold, and A. Bjarklev, "Electrically tunable bandpass filter using solid-core photonic crystal fibers filled with multiple liquid crystals," *Opt. Lett.*, vol. 35, no. 10, pp. 1608-1610, May 2010.
[41] L. Wei, J. Weirich, T. T. Alkeskjold, and A. Bjarklev, "On-chip tunable long-period grating devices based on liquid crystal photonic bandgap fibers," *Opt. Lett.*, vol. 34, no. 24, pp. 3818-3820, Dec. 2009.
[42] C. H. Lee, C. H. Chen, C. L. Kao, C. P. Yu, S. M. Yeh, W. H. Cheng, and T. H. Lin, "Photo and electrical tunable effects in photonic liquid crystal fiber," *Opt. Express*, vol. 18, no. 3, pp. 2814-2821, Jan. 2010.
[43] X. Y. Chen, F. Du, T. Guo, J. Lao, X. Zhang, Z. Zhang, F. Liu, J. Li, C. Chen and B. Guan, "Liquid crystal-embedded tilted fiber grating electric field intensity sensor," *J. Light. Technol.* vol. 35, pp. 3347C3353, Aug. 2017.
[44] Y. Liu, C. Zhao, Y. N. Zhang, G. Ma, X. Li, and Y. Zhao, "Electrically tunable optical fiber device based on hollow-core fiber infiltrated with liquid crystal," *Sensor. Actuat. A-Phys.*, vol. 318, p. 112500, Dec. 2021.
[45] X. G. Li, Y. N. Zhang, X. Zhou, and L. Cai, "Simultaneous measurement of electric field and strain with a tandem-interferometric device," *IEEE T. Instrume. Meas.*, vol. 67, no. 4, pp. 965-970, Apr. 2018.
[46] Q. Yang, S. Sun, Y. He, and R. Han, "Intense electric-field optical sensor for broad temperature-range applications based on a piecewise transfer function," *IEEE T. Ind. Electron.*, vol. 66, no. 2, Feb. 2019.

Qiang Liu received the B.S. and Ph.D. degrees from the College of Science, Yanshan University, China, in 2013 and 2018, respectively. He studied in Northeastern University, Shenyang, China from March 2015 to July 2015 as a visiting student. He is a Lecturer working in the School of Control Engineering, Northeastern University at Qinhuangdao, China. In 2018, he was awarded "Outstanding Graduate of Hebei Province, China". In 2019, he was awarded "Excellent Doctoral Thesis of Hebei Province, China". In 2020, he has been a Supervisor of Master in Northeastern University, China. From January 2020 to now, he is a Postdoctor with Faculty of Engineering and Environment, Northumbria University, Newcastle Upon Tyne, United Kingdom. His research interests include fiber optical sensors, fiber modulators, polarization filters, fiber splitters, functional materials, smart materials, photonic crystal fibers and their applications. He has authored and co-authored more than 50 scientific papers.

Pingsheng Xue received the B.S. degree from the College of Electrical Engineering, Yanshan University, China, in 2019. He is currently pursuing the master's degree with the College of Control Engineering, Northeastern University at Qinhuangdao, Qinhuangdao, China.

Qiang Wu received the B.S. and Ph.D. degrees from Beijing Normal University and Beijing University of Posts and Telecommunications, Beijing, China, in 1996 and 2004, respectively. From 2004 to 2006, he worked as a Senior Research Associate in City University of Hong Kong. From 2006 to 2008, he took up a research associate post in Heriot-Watt University, Edinburgh, U.K. From 2008 to 2014, he worked as a Stokes Lecturer at Photonics Research Centre, Dublin Institute of Technology, Ireland. He is an Associate Professor/Reader with Faculty of Engineering and Environment, Northumbria University, Newcastle Upon Tyne, United Kingdom. His research interests include optical fiber interferometers for novel optical couplers, nanofibers and sensors, microsphere sensors for bio-chemical sensing, the design and fabrication of fiber Bragg grating devices and their applications for sensing, nonlinear fibre optics, surface plasmon resonant and surface acoustic wave sensors. He has over 200 publications in the area of photonics and holds 3 invention patents. He is an Editorial Board Member of Scientific Reports, Associate Editor of IEEE Sensors Journal and Academic Editor of Journal of Sensors.

Chenyu Zhao received the B.S. degree from the College of Electrical Engineering, Zhengzhou University, China, in 2018. He is currently pursuing the master's degree with the College of Control Engineering, Northeastern University at Qinhuangdao, Qinhuangdao, China.

Yongqing Fu received the Ph.D. degree from Nanyang Technological University in 1999, Singapore, and then worked as a Research Fellow in Singapore-Massachusetts Institute of Technology Alliance, and a Research Associate in University of Cambridge. He is currently a Professor at Northumbria University, UK. He was a Reader in Thin Film Centre in University of West of Scotland, Glasgow, UK, and a lecturer in Heriot-Watt University, Edinburgh, UK. He has extensive experience in smart thin film/materials, biomedical microdevices, energy materials, lab-on-chip, micromechanics, MEMS, nanotechnology, sensors and microfluidics. He has established a worldwide reputation from his pioneer research work on shape memory films, piezoelectric thin films, nanostructured composite/films for applications in MEMS, sensing and renewable energy applications. He has authored and co-authored about 150 refereed international journal papers, one book on thin film shape memory alloys and ten book chapters in these areas. He has been regularly invited as referees for over 30 different international journals, and serves as editorial board

member for three international journals.

Wai Pang Ng received his BEng (Hons) in Communications and Electronic Engineering, from the University of Northumbria, U.K. and his Ph.D. in Electronic Engineering from University of Wales, Swansea. He is currently the Deputy Head of Department and Associate Professor of Optical Communications in the Department of Maths, Physics and Electrical Engineering, Northumbria University, U.K. and before that he was a Senior Lecturer. He has worked as Senior Networking Software Engineer at Intel Corporation. His research interests include radio-over-fiber, cognitive radio, high speed optical communications, adaptive digital signal processing and distributed fibre sensing. Dr. Ng was the Chair of IEEE UK and RI Communications Chapter (2011-2015) and the Publicity Chair of IEEE ICC2015 and ICC2016. He has also served as Guest Editor for IET Communications. He was Symposium Co-Chair of Signal Processing for Communications Symposium at ICC 2009, Technical Chair of CSNDSP 2010, Technical Chair of NOC/OCI 2011, and TPC members for numerous international conferences including GLOBECOM and ICC since 2006. He is a member of SPCE TC, TCGCC, ONTC and FiWi Sub-TC. He is also a senior member, IEEE.

Richard Binns is the Head of Department of Mathematics Physics and Electrical Engineering and Associate Professor at Northumbria University. He is currently responsible for a department of 60 staff a member of the faculty executive routinely headed up professional body accreditations and establishing collaborative links to institutions in Malaysia, Singapore and China. Dr Richard Binns graduated from Huddersfield University with a degree in Electronic and Information Engineering in 1993 and also a PhD in Analogue Test strategies in 1997. He moved to Northumbria University in 2001 on an EPSRC post-doctoral contract looking into Analogue Synthesis tool development in collaboration with Ericson Components and Cadence Design Systems. Current research works is varied from design of electronics for visible light communications, energy management in electric vehicles, research into radiation detection mechanisms for personal dosimetry and power control systems development.